Development of a Novel Underwater Robotic Platform with Rotating Thrusters for Hovering*

Sangrok Jin, Seokwoo Lee, Jihoon Kim, Jongwon Kim and TaeWon Seo

***Abstract*— There are many harmful marine organisms, such as starfishes, in underwater environments. Underwater task to eliminate such organisms by divers is dangerous and inefficient. This paper proposes a novel remotely operated vehicle (ROV) platform for a robotic application to capture harmful marine organisms. The proposed underwater robotic platform has four rotatable thrusters for hovering motion against ocean current and reaction force of manipulator. Design procedure is presented and a prototype based on the design is assembled. Dynamic model is derived and a nonlinear controller based on backstepping algorithm is synthesized. Simulation results show possibility of hovering motion that can maintain static position and orientation of robot against ocean current.**

I. INTRODUCTION

Many mobile field robots have recently been designed to carry out various tasks in difficult environments [1-3]. Mobile field robots can help workers undertake dangerous activities. The underwater is very awkward environment for human workers. Various underwater robots have been developed to perform underwater missions such as the inspection of marine ecology [4], exploration of the deep sea [5], excavation of the ocean floor [6], and inspection of submarine pipelines [7].

The southern coast of Korea has considerable trouble due to starfish, which are invasive species and are prodigious eaters. Above all, as a non-native predator, the Amur starfish, as shown in Figure 1(a), causes significant damage to shellfish. The starfish has a large appetite and very high breeding potential and regeneration. It is also a major problem that starfish has no natural enemy in the Korean Sea. The United Nations (UN) and International Maritime Organization (IMO) have listed the starfish as one of the global harmful organisms [8].

Aqua culturists and divers have continually tried to eliminate the starfishes. One diver can catch up to 100 kg of starfishes manually per day, as shown in Figure 1(b). However, this work is very hard and inefficient. Underwater task always has risk for accidents and decompression sickness. . In scuba diving, a diver can be submerged 30–40 min per air container and up to 20 m in depth. After an underwater task, some divers complain of musculoskeletal disorders, skin disease, and dysury. Korean woman divers, called "Haenyeo," are

Figure 1. a) The Amur starfish , b) Scuba divers' activity to clean up Amur starfish.

breath-holding divers. A Haenyeo can dive for one min in up to 10 m of water by holding her breath. They are suffering from chronic headaches and musculoskeletal disorders because of repeated diving for 5 to 6 hour a day [9].

Existing underwater robots can be considered for alternative of this task, but the robots are not optimized for this type of work. Most compact underwater robots have been developed only for inspection, and they have low payload. Performing particular underwater task needs hovering ability. Ocean current and reaction force from manipulator are major disturbance. Robotic platform can maintain position and orientation of robot within workspace against disturbance. Sakagami et al. [10] controlled attitude of underwater vehicle-manipulator system using rotating buoy. This system has only one degree of freedom. Doniec et al. [11] used moving battery inside robot body for control of pitch angle. It has low payload under the limit of battery weight.

This paper proposes a novel design of robotic platform which has four rotatable thrusters in order to maintain position and orientation simultaneously. For space efficiency, the four thrusters are located on a horizontal plane; a starfish-capturing manipulator or a driving-wheel can be equipped at the bottom or top of the robotic platform. Dynamic model of the robotic platform is derived, and control design is performed for nonlinear system. Finally, robot prototype is assembled based on the design.

II. PROBLEM DEFINITION

A. Conditions of the Working Environment

On the southern coast of Korea, the average depth of water in which many starfish live is up to 30 m, and the floor of the sea at a shellfish farm is relatively flat. The flow speed of the

*Research supported by The National Research Foundation (NRF) of Korea Grant funded by Korean Government (MEST) [No. 2012-0003247].

Sangrok Jin, Seokwoo Lee, Jihoon Lee, and Jongwon Kim are with the School of Mechanical and Aerospace Engineering, Seoul National University, Seoul, Korea (e-mail: rokjin@rodel.snu.ac.kr, swlee@rodel.snu.ac.kr, hoonkim@rodel.snu.ac.kr, and jongkim@snu.ac.kr).

TaeWon Seo is with the School of Mechanical Engineering, Yeungnam University, Gyeongsan, Korea (corresponding author, phone: +82-53-810-2442; fax: +82-53-810-4627; e-mail: taewon_seo@ yu.ac.kr).

current is less than 1 knot (0.5 m/s) and the transparency of the sea water is over 2.5 m [8].

The Amur starfish has a very weak adhesive force. Amur starfish cannot move quickly, so it uses water flow to move. They live in groups because of their huge population numbers.

B. *Required Specifications*

The width of robot must be less than 700 mm, the length is less than 1000 mm, and the height is less than 500 mm. In order to handle the robot for two persons without special launch equipment, weight of the robot must be below 60 kgf. The maximum payload in the water is 5 kgf. The maximum swimming speed is 2 knots (1.0 m/s). Robotic platform can maintain position and orientation of robot within workspace against ocean current and reaction force of manipulator during the underwater task.

III. PLATFORM DESIGN

A. *Mechanism Design*

As shown in Figure 2, we proposed a new underwater robotic platform using four rotating thrusters. Four thrusters are rotatable along the axial direction represented by the green line in Figure 2, and each of the two thrusters is rotated synchronously. Then, the robotic platform can achieve six degree-of-freedom motions in space, as shown in Figure 3. Each thruster can generate thrust force less than 2.2 kgf.

The mainframe is designed by the frame structure. The frame is manufactured by ABS polymer, which is denoted in blue color. Based on the frame, each part based on acrylic box is equipped. Yellow colored buoys are attached on top and bottom of the vehicle made by polypropylene (PP). Docking mechanism in the upper and lower parts of the platform is going to be used to attach a robot manipulator or other devices for capturing starfishes. The watertight performance of the whole robot body is within 5 bar pressure, corresponding to the pressure in 40 m depth.

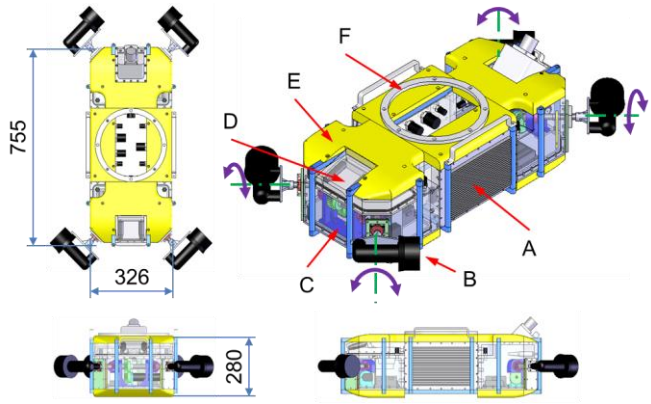

Figure 2. Mechanical configuration of the platform design. The violet arrows denote the rotatable directions of each thruster. A: DC power supply box with heat dissipation panel, B: Rotatable thrusters, C: Rotationg mechanism with bevel gears, D: Camera box with lighting, E: Buoy, F: Docking mechanism with a manipulator.

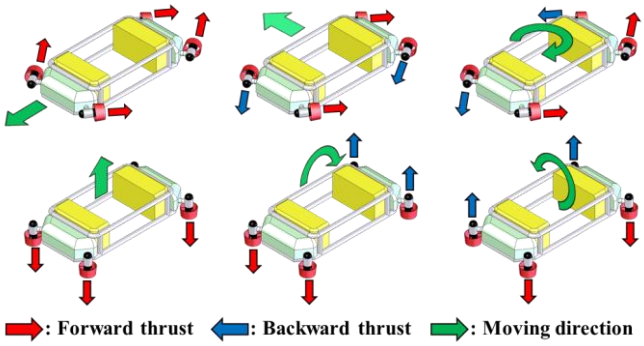

Figure 3. 6-DOF movement of the robotic platform.

TABLE I. SPECIFICATON PF COMPONENTS OF THE PLATFORM.

Components	EA	Buyer and specification
Motors and controllers		
Thrusters	4	BTD150, Seabotix
Thrust drivers	2	NT-M-DCDM2410, NTREX
Rotating servo motors	2	EC-max30, MAXON
Servo drivers	4	EPOS2 24/5, MAXON
DC power supplies	2	HWS600, TDK·Lambda
Sensors		
Camera	2	VH21HQ, VISION HITECH
Pressure transducer	1	Model 516, setra
Inetria Measuring Unit (IMU)	1	RTx, RUVA TECH

B. *Electronics and Communication*

Table I summarizes the specifications of the electronic components of the underwater platform. Two types of 12 V and 24 V power supplies are used. The vehicle is controlled by a PC-based tele-operation. The driver of the thrusters and the driver of the DC servo motors communicate through the DAC board. DC motor drivers communicate based on CAN. Final input/output (IO) RS232 signal of the platform is converted to RS485 to communicate with the external PC-based controller.

This robot control requires only 3-axis attitudes and relative position from objects as actual divers because it navigates manually by the operator. The sensorial system consists of IMU, pressure transducer for depth sensor, and two cameras. Output of IMU shows 3-axis Euler angles and pressure transducer indicates heave position. Two cameras take stereo vision in order to calculate the relative position of the robot by visual-servoing algorithm.

C. *The Prototype of an Underwater Robotic Platform*

Platform prototype is assembled as shown in Figure 4(a), and performs test diving in water tank as shown in Figure 4(b). The parameters of the prototype are summarized in Table II. Total weight of the platform is 57.1 kgf in air. Buoyancy force of the platform is set up by 57 kgf in fresh water. The robot is designed that a whole body has nearly neutral buoyancy. If the body-fixed frame is attached on intersection of diagonal line connected center of thrusters, center of gravity and center of buoyancy nearly coincide with the origin of body-fixed frame, as shown in Table II. Off-diagonal terms of inertia matrix, I_{xy},

I_{yz}, and I_{zx}, are much smaller than diagonal terms, because the body shape has three planes of symmetry.

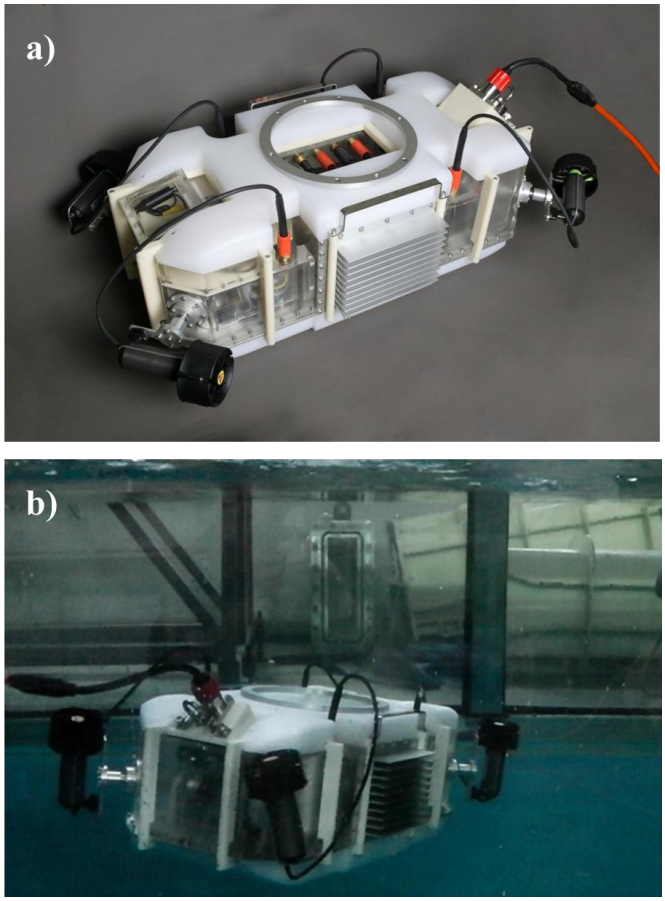

Figure 4. a) Prototype assembly of the robotic platform, b) test diving.

TABLE II. SPECIFICATON PF COMPONENTS OF THE PLATFORM.

Parameters	Values
Weight in air	W = 57.1 kgf
Buoyancy	B = 57 kgf
Moment of inertia	I_x = 1.100 kg·m^2 I_y = 3.648 kg·m^2 I_z = 4.099 kg·m^2 I_{xy} = -0.018 kg·m^2 I_{yz} = -9.662×10^{-5} kg·m^2 I_{zx} = -0.016 kg·m^2
Center of gravity	(x_G, y_G, z_G) = (-1.71 mm, -0.06 mm, 2.61 mm,)
Center of buoyancy	(x_B, y_B, z_B) = (1.33 mm, -0.42 mm, 5.83 mm)

IV. DYNAMIC MODEL

A. Equations of Motion

Generally, a 6-DOF nonlinear dynamic equation of motion in the earth-fixed reference frame is expressed as follows [12]:

$$\mathbf{M}_\eta(\eta)\ddot{\eta} + \mathbf{C}_\eta(\nu,\eta)\dot{\eta} + \mathbf{D}_\eta(\nu,\eta)\dot{\eta} + g_\eta(\eta) = \tau_\eta, \qquad (1)$$

where $\mathbf{M}_\eta$ is the inertia matrix composed of rigid body and added mass terms, $\mathbf{C}_\eta$ is the Coriolis and centripetal matrix composed of rigid body and added mass terms, $\mathbf{D}_\eta$ is the damping matrix, g_η is the gravity and buoyancy vector, τ_η is the external force and moment vector involving thrusting force vector, η is the position and orientation vector with coordinates in the earth-fixed frame, and ν is the linear and angular velocity vector with coordinates in the body-fixed frame.

B. Thruster Vector Map

The external forces and moments vector contains the thrusting force and moment vector and disturbance forces and moments as follows:

$$\tau_\eta = f_c + f_e \qquad (2)$$

where f_c is thrusting force and moment vector, and f_e is disturbance, such as ocean current and reaction force of manipulator. The thrusting force and moment vector is determined from the position and direction of the thrusters as shown in Figure 5. The f_c is derived from following vector relation:

$$f_c = \mathbf{J}^{-T}(\eta)\begin{bmatrix}\mathbf{B}(\theta_1,\theta_2) & 0_{6\times1} & 0_{6\times1}\end{bmatrix}\begin{bmatrix} f_1 \\ f_2 \\ f_3 \\ f_4 \\ \theta_1 \\ \theta_2 \end{bmatrix}, \qquad (3)$$

where **J** is the transformation matrix, **B** is thruster vector mapping matrix related through the rotation angles of thrusters.

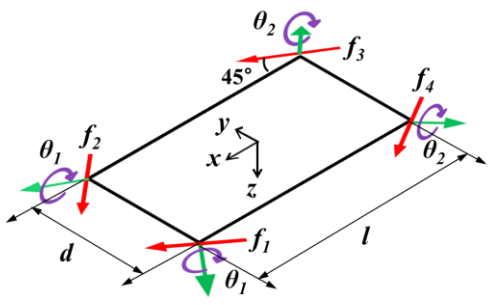

Figure 5. Configuarion of the thrusting vector.

Thruster vector map has high nonlinearity because two inputs of total six inputs, angles of thrusters (θ_1, θ_2), are included in the thruster vector mapping matrix **B** (Appendix)

V. Control Design

The objective of the robotic platform is stationary hovering motion. When displacements of position and orientation are occurred, controller calculates proper input and feeds back. A major problem is nonlinear thruster vector map. Proper solutions of input cannot be obtained because (3) has zero columns. Similar problems have been solved by differentiation on quadrotor with tilting propellers [13] and steering wheeled mobile robot [14]. This paper tries to solve the zero column problem through the backstepping control method.

Input force and moment about error of position and orientation is defined as follows:

$$f_c = -\mathbf{K}_2\dot{e} - \mathbf{K}_1 e + g_\eta(\eta) + \upsilon_e, \tag{4}$$

where $e := \eta - \eta_d$, $\dot{e} = \dot{\eta}$, $\mathbf{K}_1$, $\mathbf{K}_2$ are constant gain matrix. After substituting (4) to (1), Lyapunov candidate function is defined as follows:

$$V = \frac{1}{2}\begin{pmatrix}\dot{e}\\ e\end{pmatrix}^T \mathbf{Q}\begin{pmatrix}\dot{e}\\ e\end{pmatrix} + \frac{1}{2\gamma}\upsilon_e^T\upsilon_e, \tag{5}$$

where $\mathbf{Q} = \begin{bmatrix}\mathbf{M}_\eta & \varepsilon\mathbf{M}_\eta\\ \varepsilon\mathbf{M}_\eta & \mathbf{K}_1 + \varepsilon\mathbf{K}_2\end{bmatrix}$. Then the following backstepping control law is obtained:

$$\dot{\upsilon}_e = -\gamma(\dot{e} + \varepsilon e) - \lambda\upsilon_e. \tag{6}$$

Here, if **Q**>0, the above backstepping control can be guaranteed the stability as follows:

$$\frac{dV}{dt} = -\begin{pmatrix}\dot{e}\\ e\end{pmatrix}^T \mathbf{Q}\begin{pmatrix}\dot{e}\\ e\end{pmatrix} - \frac{\lambda}{\gamma}\upsilon_e^T\upsilon_e \le 0, \tag{7}$$

where λ, γ are nonnegative constants. Substituting (3) and (4) to (6), we can describe the derivative of input vector relation as follows:

$$\begin{aligned}&\begin{bmatrix}\mathbf{B}(\theta_1,\theta_2) & \frac{\partial\mathbf{B}}{\partial\theta_1}\bar{f} & \frac{\partial\mathbf{B}}{\partial\theta_2}\bar{f}\end{bmatrix}\begin{bmatrix}\dot{\bar{f}}\\ \dot{\theta}_1\\ \dot{\theta}_2\end{bmatrix}\\ &= \mathbf{J}^T(\eta)[-\dot{\mathbf{J}}^{-T}(\eta)\mathbf{B}(\theta_1,\theta_2)\bar{f}\\ &\quad -\mathbf{K}_2\ddot{e} - \mathbf{K}_1\dot{e} + \frac{\partial g_\eta}{\partial\eta}\dot{\eta} - \gamma(\dot{e} + \varepsilon e)\\ &\quad -\lambda\{\mathbf{J}^{-T}(\eta)\mathbf{B}(\theta_1,\theta_2)\bar{f} + \mathbf{K}_2\dot{e} + \mathbf{K}_1 e - g_\eta(\eta)\}],\end{aligned} \tag{8}$$

where $\bar{f} = [f_1 \quad f_2 \quad f_3 \quad f_4]^T$. The matrix in front of input vector has full rank, and then the solution of input can be obtained by inverting the matrix.

VI. Simulations

Simulations describe the hovering motion of a robotic platform by applying the backstepping controller on the dynamic model presented in Section IV, and ocean currents is applied in the system as the disturbance. Simulation parameters, such as the gains, are summarized in Table III.

TABLE III. Simulation Parameters.

Parameters	Values
K_1	*Diag* (10, 10, 10, 100, 100, 100)
K_2	*Diag* (17.275, 52.2, 73.25, 0.34, 2.67, 1.535)
ε	0.01
γ	10
λ	1

A. Ocean Currents

The average current velocity is generated by using a 1st-order *Gauss-Markov Process*. The current velocity V_c is described by the following differential equation [15]:

$$\dot{V}_c = \omega(t), \tag{9}$$

where $\omega(t)$ is a zero mean Gaussian white noise sequence. The velocity is limited below 0.25 m/s (0.5 knot). The earth-fixed current velocity can be related to V_c with angle of attack (α) and sideslip angle (β) describing in Figure 6, and derived as follows:

$$\begin{bmatrix}u_c^E\\ v_c^E\\ w_c^E\end{bmatrix} = \begin{bmatrix}V_c\cos\alpha\cos\beta\\ V_c\sin\beta\\ V_c\sin\alpha\cos\beta\end{bmatrix}, \tag{10}$$

where u_c^E, v_c^E, w_c^E are the earth-fixed current velocity components about *x*, *y*, *z* axes, respectively. The ocean current velocity is included in the dynamic model by making relative velocity terms [15].

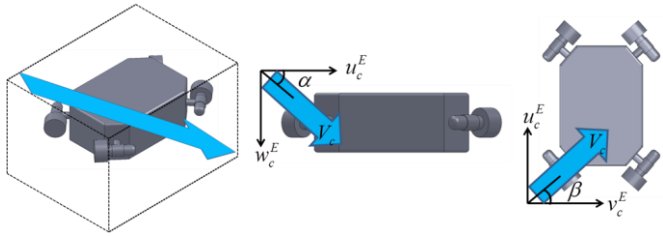

Figure 6. Orientation of the average current velocity with earth-fixed axes.

B. Simulation under Ocean Currents

In the first simulation, hovering motion is tested under ocean currents which has only sideslip angle. Desired position and orientation vector η_d is $[0\ 0\ 0\ 0\ 0\ 0]^T$, and the sideslip angle β is 45°. The second simulation is tested under ocean currents which has only angle of attack. The angle of attack α is 10°. Results of the first simulation are shown in Figure 7 (a-c): (a) is *x*-directional position, (b) is *y*-directional position, and (c) is yaw angle. Results of the second simulation are shown in Figure 7 (d-f): (d) is *z*-directional position, (e) is roll angle, and (f) is pitch angle. The angle of attack of ocean current is more influential on the robot control than the sideslip angle because of flat shape of robot body. When the angle of attack and the sideslip angle are applied in the system simultaneously, the controller cannot maintain stable state.

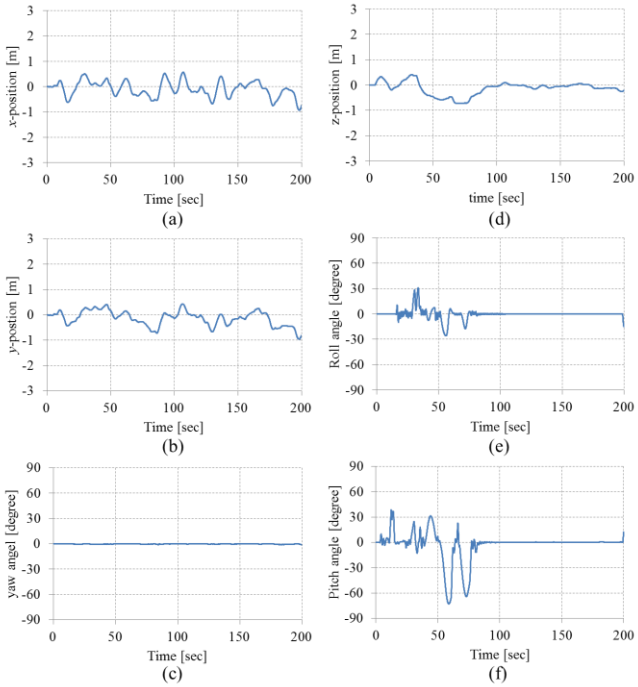

Figure 7. Position and orientaion of robot under ocean currents, results of the first simulation: (a) *x*-directonal postion, (b) *y*-directional position, (c) yaw angle, results of the secons simulation: (d) *z*-directional position, (e) roll angle, (f) pitch angle.

C. Maintain a Certain Pitch Angle under Ocean Currents

In this simulation, the maintenance ability of a certain pitch angle of robot body is tested under ocean currents. Desired position and orientation vector η_d is $[0\ 0\ 0\ 0\ \pi/6\ 0]^T$, the angle of attack α is 0°, and the sideslip angle β is 0°. The pitch angle is well controlled as shown in figure 8 (a), and the roll angle is stable as shown in figure 8 (b). However, *x*, *y*, and *z*-directional positions and yaw angle have not stable state.

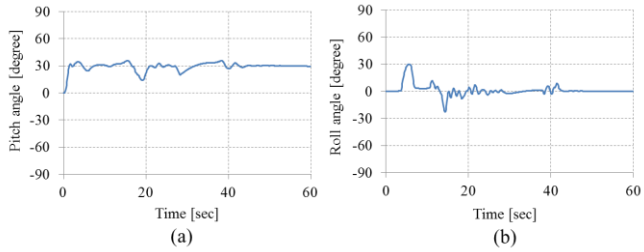

Figure 8. The results of simulation about keeping a certain pitch angle under ocean currents, (a) pitch agle, (b) roll angle.

D. Future Works

First of all, precise gain tuning is planned to be performed in order to complete the stable 6-DOF backstepping controller. On the next step, we search robust control design methods through comparing the control designs (e.g., adaptive control, sliding mode control and nonlinear H_∞ optimal control). Then, experiments are going to be performed real underwater. Design and assembly of a capturing manipulator is also very important to achieve the main goal of the research.

VII. Conclusion

In this paper, a novel underwater robot with four rotating thruster is proposed. Rotating thruster mechanism achieves 6-DOF motion for hovering with four thrusters. The prototype of robot was manufactured, and the basic performance was tested. Through dynamic modeling, motion equation and nonlinear thrusting vector was derived. High nonlinearity of rotating thrusters was controlled based on backstepping control technique. Simulations showed the hovering ability of robot against ocean currents. In the results of simulations, each 3-DOF combination (*x*, *y*, yaw / *z*, pitch, roll) is well controlled, but whole 6-DOF control is not yet stable. We expect the existing problem can be solved by precise gain tuning or applying another control design methodologies.

Appendix

The thruster vector mapping matrix B in Section IV. is derived as follows:

$$\mathbf{B}(\theta_1,\theta_2)=\begin{bmatrix} \frac{\cos\theta_1}{\sqrt{2}} & \frac{\cos\theta_1}{\sqrt{2}} & \frac{\cos\theta_2}{\sqrt{2}} & \frac{\cos\theta_2}{\sqrt{2}} \\ \frac{\cos\theta_1}{\sqrt{2}} & -\frac{\cos\theta_1}{\sqrt{2}} & \frac{\cos\theta_2}{\sqrt{2}} & -\frac{\cos\theta_2}{\sqrt{2}} \\ -\sin\theta_1 & -\sin\theta_1 & -\sin\theta_2 & -\sin\theta_2 \\ \frac{d\sin\theta_1}{2} & -\frac{d\sin\theta_1}{2} & -\frac{d\sin\theta_2}{2} & \frac{d\sin\theta_2}{2} \\ \frac{l\sin\theta_1}{2} & \frac{l\sin\theta_1}{2} & -\frac{l\sin\theta_2}{2} & -\frac{l\sin\theta_2}{2} \\ \frac{l+d}{2\sqrt{2}}\cos\theta_1 & -\frac{l+d}{2\sqrt{2}}\cos\theta_1 & -\frac{l+d}{2\sqrt{2}}\cos\theta_2 & \frac{l+d}{2\sqrt{2}}\cos\theta_2 \end{bmatrix},$$

where l is length of a robot, d is width of a robot, and θ_1, θ_2 are rotating angles.

REFERENCES

[1] Sutoh M., Nagaoka K., Nagatani K., Yoshida K. , "Evaluation of influence of surface shape of locomotion mechanism on traveling performance of planetary rovers," *Robotics and Automation (ICRA), 2012 IEEE International Conference on* , pp.3419-3424.

[2] Khan Y.N., Masselli A., Zell A. , "Visual terrain classification by flying robots," *Robotics and Automation (ICRA), 2012 IEEE International Conference on*, pp.498-503.

[3] Ma J., Susca S., Bajracharya M., Matthies L., Malchano M., Wooden D. , "Robust multi-sensor, day/night 6-DOF pose estimation for a dynamic legged vehicle in GPS-denied environments," *Robotics and Automation (ICRA), 2012 IEEE International Conference on* , pp.619-626.

[4] H. Hu, "Biologically Inspired Design of Autonomous Robotic Fish at Essex*," in Proc. of the IEEE SMK UK-RI Chapter Conf. on Adv. in Cybernetic Systems*, pp. 1–8, 2006.

[5] M. Murashima, H. Nakajoh, et al., "7,000 m class ROV KAIKO7000," *in OCEANS'04. MTTS/IEEE TECHNO-OCEAN'04*, vol. 2, pp. 812–817.

[6] C. Revillon. (2005, May). "Nexans innovative Spider dredging system, levels the seabed at depths of 1,000 m before laying cables." [Online]. Available: http://www.nexans.ru/

[7] D. Krys and H. Najjaran, "Development of Visual Simultaneous Localization and Mapping (VSLAM) for a Pipe Inspection Robot," *in Proc. Of the 2007 IEEE International Symposium on Computational Intelligence in Robotics and Automation*, pp. 344-349, 2007.

[8] S. Jin, S. Lee, J. Kim and T. Seo, "Starfish capture robotic platform: conceptual design and analysis," *Journal of the Korean Society for Precision Engineering*, vol. 29, no. 9, pp. 978-985, 2012.

[9] G. Sa, S. Yoon, K. Lee, T. Hwang, and S. Lee, "Incidence, prevalence, and prevention of diving related disease of diving fisherman and breath-hold divers in Korea," *Korean Ministry of Maritime Affairs and Fisheries*, Korea, December 2006.

[10] Sakagami N., Shibata M., Kawamura S., Inoue T., Onishi H., Murakami S., "An attitude control system for underwater vehicle-manipulator systems," *Robotics and Automation (ICRA), 2010 IEEE International Conference on*, pp.1761-1767.

[11] Doniec M., Vasilescu I., Detweiler C., Rus D. , "Complete SE3 underwater robot control with arbitrary thruster configurations," *Robotics and Automation (ICRA), 2010 IEEE International Conference on* , pp.5295-5301.

[12] Thor I. Fossen, *Guidance and Control of Ocean Vehicles*. University of Trondheim, Norway: John Wiley & Sons, 1994, ch.4.

[13] Markus Ryll, Heinrich H. Bülthoff, Paolo Robuffo Giordano, "Modeling and control of a quadrotor UAV with tiling propellers," *Robotics and Automation (ICRA), 2012 IEEE International Conference on*, pp. 4606-4613.

[14] Alessandro De Luca, Giuseppe Oriolo, Paolo Robuffo Giordano, "Kinematic control of nonholonomic mobile manipulators in the presence of steering wheels," *Robotics and Automation (ICRA), 2010 IEEE International Conference on*, pp. 1792-1798.

[15] Thor I. Fossen, *Guidance and Control of Ocean Vehicles*. University of Trondheim, Norway: John Wiley & Sons, 1994, ch.3.